Self-bound droplets of light with orbital angular momentum

Niclas Westerberg,[1,*] Kali E. Wilson,[1] Callum W. Duncan,[1] Daniele Faccio,[1,2,3] Ewan M. Wright,[1,3] Patrik Öhberg,[1] and Manuel Valiente[1,†]

[1]*Institute of Photonics and Quantum Sciences, Heriot-Watt University, SUPA, Edinburgh EH14 4AS, United Kingdom*
[2]*School of Physics & Astronomy, University of Glasgow, SUPA, Glasgow G12 8QQ, United Kingdom*
[3]*College of Optical Sciences, University of Arizona, Tucson, Arizona 85721, USA*

(Received 8 February 2018; published 21 November 2018)

Systems with competing attractive and repulsive interactions have a tendency to condense into droplets. This is the case for water in a sink, liquid helium, and dipolar atomic gases. Here we consider a photon fluid which is formed in the transverse plane of a monochromatic laser beam propagating in an attractive (focusing) nonlocal nonlinear medium. In this setting we demonstrate the formation of the optical analog of matter-wave droplets and study their properties. The system we consider admits droplets that carry orbital angular momentum. We find bound states possessing liquidlike properties, such as bulk pressure and compressibility. Interestingly, these droplets of light, as opposed to optical vortices, form due to the competition between long-range s-wave (monopole) and d-wave (quadrupole) interactions as well as diffraction.

DOI: 10.1103/PhysRevA.98.053835

I. INTRODUCTION

Droplet formation is ubiquitous in nature, its occurrence ranging from classical fluids, such as liquid water in normal conditions, to quantum many-body systems, such as liquid helium [1] or atomic mixtures [2–5]. In either scenario, the stabilization of droplets, which are self-bound states, is typically driven by the competition between attractive and repulsive forces between the microscopic constituents of the system. In quantum mechanics, purely attractive forces may still favor droplet formation due to quantum effects. This is the case for zero-range interacting bosonic systems in the universal and few-body limit at zero temperature in two spatial dimensions [6,7]. Renormalization effects in the only coupling constant of the system provide the necessary length scale, closely linked to the droplet's size, which in turn provide a mechanism for stabilization of quantum droplets. More recently, droplets and gas-liquid or gas-droplet transitions in (dipolar) atomic systems have been observed in several groundbreaking experiments [2–4,8,9]. Although the stabilization mechanism in dipolar atomic systems is due to purely quantum-mechanical beyond-mean-field effects [10–14] that require large particle numbers, three- and many-body forces are known to be capable of stabilizing droplets in an otherwise collapsing system [15,16] and may be the reason for the liquid to Luttinger liquid transition in one-dimensional ^{4}He [17]. In addition, we should note that the quantum-mechanical stabilization can be modeled by a classical potential in the effective-field-theory sense, as is done in Ref. [3].

The most prominent example of natural quantum droplets is large nuclei, some of which have a ground state and part of their excitations well accounted for by the liquid drop model [18]. Droplet formation is however also present in many other systems, with both local and nonlocal (e.g., power-law) interactions [2–4,6,11,12,16,19,20]. In the context of atomic matter waves and nonlinear optics, solitons, not droplets, are a much more common phenomenon and have been observed in a variety of scenarios (see Refs. [21–24] and references therein). Solitons are stationary states that arise in *integrable* systems from the balance between the kinetic energy (i.e., diffraction) and nonlinear interactions. For these to be stable, fine-tuned shapes and densities are required. Droplets, on the other hand, are dynamical objects that can be defined as self-bound finite-size objects that are stable against perturbations in size, shape, and density due to a competition of attractive and repulsive forces. This is the definition we will use hereafter.

The connection between droplets and solitons in nonlinear optics has been highlighted by Michinel *et al.* [25,26], who showed the formal analogy between bosons with competing two- and three-body forces and light in cubic-quintic nonlinear media, forming what they called liquid light. Moreover, in the context of long-range interactions, similar states have been referred to as nonlocal solitons [27–42], dipole solitons [43–45], and when rotations are present, azimuthons [46].

In this work we draw the connection between matter-wave droplets and bound states in nonlinear optics with orbital angular momentum (OAM) aiming to explain the underlying mechanisms of the latter. Using the language of atomic quantum fluids, we investigate the properties, underlying mechanisms of formation, and the dynamics of these bound states in detail. We show that they are stable against size and shape perturbations due to a competition between long-range s-wave and d-wave forces. While the competing forces are of a different form compared to that of atomic liquids, we nonetheless find that liquidlike properties, such as bulk pressure, compressibility, and a speed of sound can be defined in the system.

*nkw2@hw.ac.uk
†M.Valiente_Cifuentes@hw.ac.uk

The paper is structured as follows. In Sec. II we define the optics–matter-wave analogy, followed by Sec. III, where the pseudoenergy of bound states is calculated and a different type of expansion for long-range interactions is introduced. In Sec. IV we specifically consider the p-wave state, the liquidlike properties of which are explored in Sec. V. The dynamics of a perturbed p-wave state is then explored in Sec. VI. We summarize in Sec. VII.

II. OPTICS–MATTER-WAVE ANALOGY

We consider the transverse plane of a monochromatic laser field, for which the photons are effectively massive and two dimensional. Nonlinearities can be induced by a nonlinear optical medium in such a way that a photon fluid is formed where superfluidity has also been observed with a repulsive (defocusing) nonlinearity [47–51]. Here the direction of propagation z plays the role of time t in quantum mechanics. We concentrate on nonlocal photon fluids [52–54], where the nonlinearity is long range, formed in the transverse plane of a laser beam propagating in a thermo-optic medium, for which the change in refractive index Δn is induced by heat absorption in the medium. Importantly, we are interested in systems with an attractive (focusing) nonlinearity. Superfluid behavior is thus not expected. As we will show, liquidlike behavior is however present. We will work with slowly varying electric-field envelopes $E(\mathbf{r}, z)$, well described within the paraxial approximation to the wave equation [55],

$$i\frac{\partial E}{\partial z} = -\frac{1}{2k_0}\nabla^2 E - \frac{k_0}{n_0}\Delta n E - \frac{i\alpha}{2}E \equiv \mathcal{H}_*, \tag{1}$$

where ∇^2 is the Laplacian in the transverse plane [$\mathbf{r} = (x, y)$]. In Eq. (1), the wave number k_0 is given by $k_0 = 2\pi n_0/\lambda$, with n_0 the background refractive index of the medium and λ the wavelength of the beam, while α is the linear absorption coefficient of the medium. The change in refractive index Δn is a nonlinear functional of the electric-field envelope

$$\Delta n[E, E^*] = \gamma \int d^2r' R(\mathbf{r} - \mathbf{r}')|E(\mathbf{r}', z)|^2, \tag{2}$$

where $\gamma = \alpha\beta\sigma^2/\kappa$, with β, κ, and σ the thermo-optic coefficient, thermal conductivity, and nonlocal length of the medium (set by the physical size), respectively, and $R(\mathbf{r})$ the medium's thermo-optical response function [53,54,56]. The response function of the nonlinear medium is well approximated using the distributed loss model, which gives $R(\mathbf{r}) = K_0(|\mathbf{r}|/\sigma)/2\pi\sigma^2$ [54], with K_0 the modified Bessel function of the second kind of order zero.

The analogy between matter waves and nonlinear optics is drawn by identifying E with the condensate order parameter ψ, and γR with the interaction potential V. Full analogy with a closed atomic system is achieved for negligible absorption α, which is the situation we consider here. As we will see, both pseudoenergy H_* and pseudochemical potential μ_* arise from the conserved quantities of the photon fluid, which will be defined analogously to matter waves. It is easy to see that Eq. (1), neglecting absorption, can be obtained by minimizing the following Lagrangian density with respect to E^*:

$$\mathcal{L} = E^*\left(i\partial_z + \frac{\nabla^2}{2k_0} + \frac{k_0}{2n_0}\Delta n\right)E. \tag{3}$$

Naturally, due to the z-translational invariance of $\mathcal{L}$, the Hamiltonian

$$H_* = \int d^2r\, E^*\left(-\frac{\nabla^2}{2k_0} - \frac{k_0}{2n_0}\Delta n\right)E \tag{4}$$

$$= \int d^2r\left(\frac{1}{2k_0}\nabla E^*(\mathbf{r}, z)\cdot\nabla E(\mathbf{r}, z) - \frac{k_0}{2n_0}\Delta n(\mathbf{r}, z)E^*(\mathbf{r}, z)E(\mathbf{r}, z)\right) \tag{5}$$

is a conserved quantity. We will refer to Eq. (4) as the pseudoenergy of the photon fluid, in analogy to matter waves. Importantly, another conserved quantity is the power P, which will play the role of the number of atoms N. That is,

$$P = \int d^2r\, |E(\mathbf{r}, z)|^2 \tag{6}$$

is constant in propagation. We can now define the pseudochemical potential μ_* by minimising the pseudoenergy with Eq. (6) as a constraint. In other words, we want to minimise

$$X[E^*(\mathbf{r}, z), E(\mathbf{r}, z)] = H_* - \mu_* \int d^2r\, E^*(\mathbf{r}, z)E(\mathbf{r}, z). \tag{7}$$

Using the pseudoenergy as defined through Eq. (4), we find

$$\frac{\delta X}{\delta E^*} = -\frac{1}{2k_0}\nabla^2 E - \frac{k_0}{n_0}\Delta n E - \mu_* E = 0 \tag{8}$$

and thus we can define the pseudochemical potential by

$$\mu_* E = \left[-\frac{1}{2k_0}\nabla^2 - \frac{k_0}{n_0}\Delta n\right]E = \mathcal{H}_* E, \tag{9}$$

where $\mathcal{H}_*$ is the pseudoenergy density. This can also be seen as the eigenvalue of the Hamiltonian-density operator $\mathcal{H}_*$ and as such we can make the *Ansatz* $E(\mathbf{r}, z) = E(\mathbf{r})e^{-i\mu_* z}$ to obtain the original equation of motion in Eq. (1). From this treatment, it also follows that

$$\mu_* = \frac{\partial H_*}{\partial P}, \tag{10}$$

similarly to the chemical potential of a condensate, but where $P \to N$. Note that this is *not* a chemical potential with respect to the number of photons, but with respect to the power contained in the beam. It represents the amount of pseudoenergy you add to the system by increasing the power by an infinitesimal amount δP.

III. PSEUDOENERGY OF BOUND STATES

We are interested in bound states and will use an *Ansatz* that generalizes the nonrotating results of Hammer and Son [6]. As we will see, in the process of evaluating the pseudoenergy, we will develop a different type of expansion for highly nonlocal interactions.

For the ground state we have $E(\mathbf{r}, z) = E_p(\mathbf{r})\exp(-i\mu_* z)$, with μ_* the pseudochemical potential.

The power-normalized *Ansatz* takes the form

$$E_p(\mathbf{r}) = \frac{\sqrt{P}}{\sqrt{C_r C_\phi}\xi} f(r/\xi)\Phi(\phi), \tag{11}$$

where ξ is a length scale associated with the radial size of the bound state, f is a real-valued radial function, and Φ encodes the angular dependence. The normalization constants are $C_r = \int_0^\infty ds\, s f^2(s)$ and $C_\phi = \int_0^{2\pi} d\phi |\Phi(\phi)|^2$. In the following, we work with angular functions Φ that only contain $\ell = \pm 1$ OAM, that is, $\Phi(\phi) = \exp(i\phi) + \delta \exp(-i\phi)$, with δ a dimensionless constant. In other words, δ is the ratio of OAM $\ell = -1$ to OAM $\ell = 1$. We will now proceed to evaluate the Hamiltonian term by term for the bound-state *Ansätze* of the form (11), as through this we will ultimately find stable shape and size configurations in the usual variational manner. Note that in this, the shape function $f(s)$ is a functional variational parameter.

A. Kinetic pseudoenergy

Let us start with the kinetic part of the pseudo-Hamiltonian (4). We want to calculate the expectation value of the pseudoenergy $\langle \mathcal{H}_* \rangle$, using Eq. (11) as an *Ansatz*. This yields

$$H_*^{(1)} = \frac{P}{2k_0 C_r \xi^2}\left[A_1 + \frac{A_2 A_m}{C_\phi}\right] = \frac{P C_1}{2k_0 \xi^2}, \tag{12}$$

with dimensionless constants defined as $A_1 = \int_0^\infty ds\, s(\frac{df}{ds})^2$, $A_2 = \int_0^\infty ds(\frac{f^2}{s})$, $A_m = \int_0^{2\pi} d\phi |\frac{d\Phi}{d\phi}|^2$, and $C_1 = \frac{1}{C_r}[A_1 + \frac{A_2 A_m}{C_\phi}]$. Here A_1 and A_m originate from the usual Laplacian of the kinetic Hamiltonian and A_2 accounts for the centrifugal barrier.

B. Interaction pseudoenergy

As we will see in the following, analytically solving the necessary integrals for the expectation value of the pseudoenergy, in Eq. (4), with *Ansätze* of the form in Eq. (11), is not possible due to the form of the nonlocal response function R. In our case, the bound state is tightly bound [i.e., $\sigma \gg \xi$; see Fig. 1(a)] and the commonly used low-energy (gradient) expansion of R is therefore not appropriate.

Nonetheless, let us first consider the nonlocal refractive index (2) in the $\sigma \ll \xi$ limit, in order to gain some intuition. Also, let us denote the intensity, or power density, as $\rho_p(\mathbf{r}) = |E_p(\mathbf{r})|^2$. It follows that

$$\begin{aligned}\Delta n(\mathbf{r}) &= \gamma \int \frac{d^2k}{(2\pi)^2} e^{-i\mathbf{k}\cdot\mathbf{r}} R(\mathbf{k})\rho_p(\mathbf{k}) \\ &= \gamma \int \frac{d^2k}{(2\pi)^2} e^{-i\mathbf{k}\cdot\mathbf{r}} \frac{\rho_p(\mathbf{k})}{1+\sigma^2 k^2} \\ &\simeq \gamma \int \frac{d^2k}{(2\pi)^2} [1-\sigma^2 k^2] e^{-i\mathbf{k}\cdot\mathbf{r}} \rho_p(\mathbf{k}) \\ &= \left[\gamma + \gamma\sigma^2 \nabla_r^2\right]\rho_p(\mathbf{r}),\end{aligned} \tag{13}$$

where the first step follows from the Fourier transform of the modified Bessel function K_0. This is called the effective range expansion in scattering theory [57], or pionless effective-field theory in nuclear physics [58], and is valid for nonlocal interaction lengths σ much smaller than the characteristic condensate size ξ. Physically, this low-energy expansion assumes that the exchange momentum carried by $R(\mathbf{k})$ is much smaller than the condensate momentum $\rho_p(\mathbf{k})$.

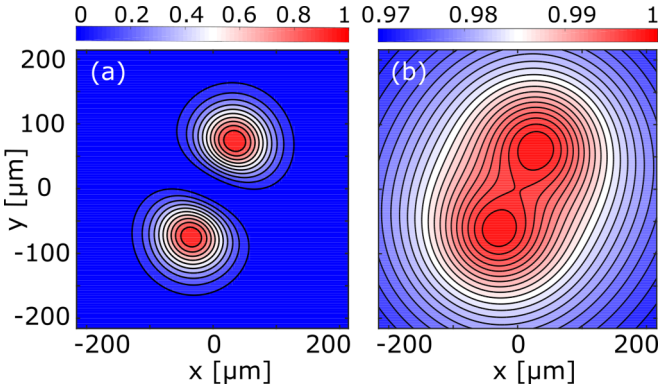

FIG. 1. (a) Normalized intensity of a p-wave droplet at $P = 1$ W input power and an equal superposition of $\ell = \pm 1$ orbital angular momentum. (b) Corresponding normalized nonlocal interaction potential Δn.

However, we are interested in the $\sigma \gg \xi$ regime. We can nonetheless do a similar expansion, which we detail below. We still consider the momentum space picture. As $\sigma \gg \xi$, it follows from line 2 of Eq. (13) that the exchange momentum k is effectively amplified by the nonlocal length. Therefore, the momentum integral is dominated by $R(\mathbf{k})$ and we may use a low-momentum expansion for the photon fluid momentum $\rho_p(\mathbf{k})$. This translates to an effective multipole expansion of the nonlocal refractive index

$$\begin{aligned}\Delta n(\mathbf{r}) &= \gamma \int \frac{d^2k}{(2\pi)^2} e^{-i\mathbf{k}\cdot\mathbf{r}} R(\mathbf{k})\rho_p(\mathbf{k}) \\ &= \int \frac{d^2k}{(2\pi)^2} e^{-i\mathbf{k}\cdot\mathbf{r}} R(\mathbf{k}) \int d^2r' e^{i\mathbf{k}\cdot\mathbf{r}'} \rho_p(\mathbf{r}') \\ &= \gamma \int d^2r' \left[1 - x'_\alpha \partial_r^\alpha + \frac{1}{2} x'_\alpha x'_\beta \partial_r^\alpha \partial_r^\beta\right]\rho_p(\mathbf{r}') \\ &\quad \times \int \frac{d^2k}{(2\pi)^2} R(\mathbf{k}) e^{-i\mathbf{k}\cdot\mathbf{r}} \\ &= \gamma\left[P - d_\alpha \partial_r^\alpha + \frac{1}{2} Q_{\alpha\beta}\partial_r^\alpha \partial_r^\beta\right] R(\mathbf{r}).\end{aligned} \tag{14}$$

We will refer to this expansion as the long-wavelength approximation (LWA).[1] Here we expand the plane wave $e^{i\mathbf{k}\cdot\mathbf{r}'}$ to identify the relevant momentum modes that contribute to the nonlocal refractive index. We should note that in order to make an accurate approximation, our reference coordinate system must be aligned with the droplet. Also, a prime implies the primed coordinates, $\partial_r^\alpha = \frac{\partial}{\partial x'_\alpha}$, and a (+,+) Einstein summation is implied. For this expansion, we have defined the

[1]Note that we can connect this to the Snyder-Mitchell approximation as this amounts to only keeping the s-wave term in the LWA and then further approximating the medium response as a quadratic.

dipole moment

$$d_\alpha = \int d^2r' x'_\alpha \rho_p(\mathbf{r}') \tag{15}$$

and the quadrupole moment

$$Q_{\alpha\beta} = \int d^2r' x'_\alpha x'_\beta \rho_p(\mathbf{r}'). \tag{16}$$

The dipole moment of the *Ansatz* in Eq. (11) vanishes identically ($\mathbf{d} = \mathbf{0}$). The quadrupole moment, on the other hand, is nonzero along its diagonal. Substituting the *Ansatz* (11) into the definition of the quadrupole moment, we obtain

$$Q_{\nu,\nu} = \frac{P\xi^2}{C_r C_\phi} Q_r q_{\nu,\nu},$$

where we have defined $Q_r = \int_0^\infty ds\, s^3 f^2(s)$, $q_{1,1} = \int_0^{2\pi} d\phi \cos^2\phi |\Phi(\phi)|^2$, and $q_{2,2} = C_\phi - q_{1,1}$. In total, we find that the self-induced refractive index is given by

$$\begin{aligned}\Delta n(\mathbf{r}) = {} & \gamma P \frac{K_0(r/\sigma)}{2\pi\sigma^2} + \gamma Q_{12} \sin(2\phi) \frac{K_2(r/\sigma)}{2\pi\sigma^4} \\ & + \frac{\gamma Q_{11}}{2}\left[\frac{\cos^2(\phi) K_0(r/\sigma)}{2\pi\sigma^4} + \frac{\cos(2\phi) K_1(r/\sigma)}{2\pi\sigma^3 r}\right] \\ & + \frac{\gamma Q_{22}}{2}\left[\frac{\sin^2(\phi) K_0(r/\sigma)}{2\pi\sigma^4} - \frac{\cos(2\phi) K_1(r/\sigma)}{2\pi\sigma^3 r}\right].\end{aligned} \tag{17}$$

Note that the d-wave term (proportional to Q_{ij}) can take negative values, providing an effective repulsion mechanism, and thus the competing forces that promote stable droplet formation, in stark contrast with the s-wave case.

Finally, we can use Eq. (17) together with our droplet *Ansatz* (11) to evaluate the nonlocal interaction part of the Hamiltonian ($H_*^{(2)}$), yielding

$$\begin{aligned} H_*^{(2)} = {} & -\frac{k_0}{2n_0}\int d^2r\, \Delta n(\mathbf{r}) |E_p(\mathbf{r})|^2 \\ = {} & -\frac{k_0 P\gamma}{2n_0 C_r C_\phi}\left\{\frac{P C_\phi Q_r^{K_0}(\xi,\sigma)}{2\pi\sigma^2} + \frac{P\xi^2 Q_r Q_r^{K_0}(\xi,\sigma)}{4\pi\sigma^4 C_r C_\phi}\right. \\ & \times\left[q_{11}^2 + q_{22}^2\right] + \frac{P\xi Q_r (Q_\phi^{\cos})^2 Q_r^{K_1}(\xi,\sigma)}{4\pi\sigma^3 C_r C_\phi} \\ & \left. + \frac{P\xi q_{12} Q_r Q_\phi^{\sin} Q_r^{K_2}(\xi,\sigma)}{2\pi\sigma^4 C_r C_\phi}\right\}, \end{aligned} \tag{18}$$

where we have defined the dimensionless constants $Q_r = \int_0^\infty ds\, s^3 f^2(s)$, $q_{11} = \int_0^{2\pi} d\phi \cos^2(\phi)|\Phi(\phi)|^2$, $q_{22} = \int_0^{2\pi} d\phi \sin^2(\phi)|\Phi(\phi)|^2$, $Q_\phi^{\cos} = \int_0^{2\pi} d\phi \cos(2\phi)|\Phi(\phi)|^2$, and $Q_\phi^{\sin} = \int_0^{2\pi} d\phi \sin(2\phi)|\Phi(\phi)|^2$, as well as the dimensionless functions $Q_r^{K_0}(\xi,\sigma) = \int_0^\infty ds\, s K_0(s\xi/\sigma) f^2(s)$, $Q_r^{K_1}(\xi,\sigma) = \int_0^\infty ds\, K_1(s\xi/\sigma) f^2(s)$, and $Q_r^{K_2}(\xi,\sigma) = \int_0^\infty ds\, s K_2(s\xi/\sigma) f^2(s)$. We explore the regions of validity for this approximation in Appendix A.

IV. STABLE CONFIGURATIONS

We have now developed a variational expression for the pseudoenergy for bound state *Ansätze*. Let us in this section explore the physics further and discuss stable bound states. For the case of zero OAM, the ground state of the pseudoenergy functional, after fixing the average power $P = \langle |E|^2 \rangle$ (or particle number in the matter-wave language), is a single circular bound state. This is well approximated by the model of Snyder and Mitchell [27] in which the nonlinear refractive index is given by a parabolic function. For reasons that will become apparent, we will refer to this as the s-wave bound state.

With nonzero OAM, however, the ground state is no longer that of the s-wave state and as we will show in this section that the system instead settles to a symmetry-protected stable state which at a first glance looks like that of two distinct lobes. This state, however, truly is a single bound state and we will refer to it as a p-wave bound state. Such a state cannot be described within the Snyder-Mitchell framework. Since our system conserves angular momentum, superpositions of $\ell = \pm 1$ modes of the electric field cannot transition into the trivial s-wave state in the absence of any perturbations. In the case of an equal superposition of $\ell = +1$ and $\ell = -1$ modes, which has zero OAM, the p-wave state is nonetheless stable as it carries a different symmetry than the s-wave state. This state also cannot fly apart, as the interaction length is much larger than the typical distance between the lobes. Therefore, if these superpositions can find a stable pseudoenergy minimum, they will form bound states that are experimentally feasible to observe. To show that this is the case, we perform a Wick rotation $z \to i\tau$ in the wave equation (1) and solve it with initial conditions of the type $E(\mathbf{r}, 0) \propto E(r)[e^{i\phi} + \delta e^{-i\phi}]$.

In Fig. 1(a) we present the result of imaginary time propagation of Eq. (1) for the intensity distribution with input power $P = 1$ W, showing that indeed the stable pseudo-ground-state configuration is a p-wave self-bound state. The formation of the bound state can be attributed to the formation of a double-well-like potential Δn, as seen in Fig. 1(b). There are two significant features that we immediately infer from Fig. 1(a). First, the zero at the origin is a consequence of the centrifugal barrier $\sim \ell(\ell+1)/r^2$. Second, the two-lobe structure suggests that the stable configuration has an equal, in absolute value, superposition of $\ell = \pm 1$ modes. Pure $\ell = 1$ or $\ell = -1$ modes would exhibit a ringlike intensity pattern, which we will show is unstable in the following.

We choose $f(s) = se^{-s}$ in Eq. (11), where we have verified that this exponential form gives lower pseudoenergy in the d-wave channel than a variety of other forms such as Gaussian functions. In Fig. 2 we show the energy landscape produced by the *Ansatz* (11) as a function of $|\delta|$ and ξ. As can be clearly observed in Fig. 2, the minimum of pseudoenergy occurs at $|\delta| = 1$ (zero-net OAM), indicating the formation of a two-peaked intensity pattern, while the ring-shaped pure ± 1 OAM ($|\delta| = 0$) configuration has the highest energy and is highly unstable. We note here that the Snyder-Mitchell approximation gives the minimum of pseudoenergy for $|\delta| = 0$, discussed in Appendix B, in stark contrast with numerical simulations and variational calculations within the LWA (see Fig. 2 and also Ref. [37]). We point out that the d-wave quadrupole term is in competition with the s-wave monopole term. This is the competition of forces that promotes liquidlike behavior.

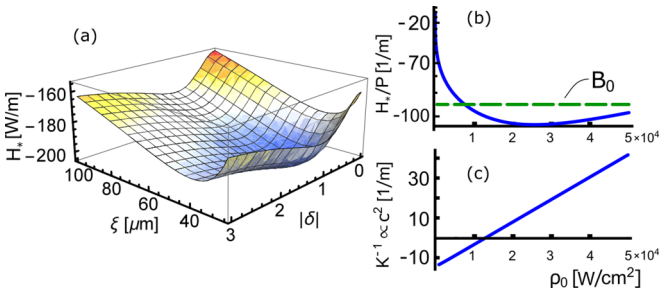

FIG. 2. (a) Pseudoenergy surface of the droplet as a function of the droplet size ξ and $|\delta|$ as given by H_* for $P = 2$ W. Note the global minimum at $|\delta| = 1$ and at the finite size $\xi = \xi_*$. (b) Pseudoenergy per unit power (blue solid line) and binding energy contribution (green dashed line) for $P = 2$ W and $|\delta| = 1$ as a function of bulk density (peak power). (c) Corresponding inverse compressibility K^{-1}.

V. LIQUIDLIKE PROPERTIES

As alluded to earlier, liquidlike features emerge in this system. The pseudoenergy per unit power (EOP), analogous to energy per particle, has a minimum at bulk density (i.e., peak intensity) $\rho_* = P/C_r C_\phi \xi_*^2$, where ξ_* is the value of ξ at the pseudoenergy minimum observed in Fig. 2(a). This can be seen in Fig. 2(b). Expanding around this minimum up to quadratic order in peak intensity $\rho_0 = P/C_r C_\phi \xi^2$, we find the EOP

$$\frac{H_*}{P} = -|B_0| - \frac{3\pi C_\phi}{16 k_0 P}\rho_0 + \frac{9\pi C_\phi^2 n_0}{64 k_0^3 \gamma P^3}\sigma^2 \rho_0^2, \qquad (19)$$

where B_0 is analogous to the binding energy[2] of the bound state at zero density with respect to the $(P-1)$-particle threshold in the many-particle language. This gives us direct insight into the formation mechanism: Local interactions in the system give rise to the linear term, promoting collapse, which is stabilized by effects related to the nonlocal interaction range (σ) in the quadratic term. Since our system is dynamical, as opposed to ultracold atomic gases which are cooled to their ground states, the relevant quantity is the EOP (19) and not an equation of state. In other words, our system may be prepared near its pseudo-ground-state configuration with a bulk density $\rho_0 \neq \rho_*$. The form of the EOP in Eq. (19) at low peak intensity is identical to the form of the equation of state found for liquid helium [1,17] and corresponds to the mean-field approximation with zero-range two-body and three-body forces. It differs only slightly from dipolar Bose-Einstein condensates (BECs) where $\rho_0^2 \to \rho_0^{3/2}$.[3]

Furthermore, from the EOP, we can define a (pseudo)bulk pressure $\mathcal{P} = \rho_0^2 \partial_{\rho_0}[H_*/P]$ and compressibility $K = (\partial_{\rho_0}\mathcal{P})^{-1}$. Zero bulk pressure gives the condition for the bound-state energy (minimum). From the compressibility, the inverse of which is plotted in Fig. 2(c), we can obtain a spinodal decomposition point [59], after which sound waves can propagate in the system. Prior to this point, the system is unstable and droplet nucleation is expected.

We have shown that this p-wave bound state not only forms due to a competition of forces, but also attains liquidlike properties. It is thus apparent that it is a droplet, and we will from here on refer to the state as a p-wave droplet in analogy with quantum many-body systems.

VI. DYNAMICS

In order to compare our theoretical variational calculation within the LWA to exact numerical simulations we need to study the dynamical (z-dependent) problem. To do so, we first modify the *Ansatz* to account for its nontrivial z dependence. For our dynamical variational parameter $\xi(z)$ (note that by conservation of angular momentum $|\delta|$ is fixed and the variational analysis is degenerate with respect to the phase of δ), we see that in order to obtain kinetic terms in the Lagrangian $L = \int d^2 r \mathcal{L}$ of the form $\sim \partial_z^2 \xi$, we need to include a phase term such that the variational *Ansatz* becomes

$$E_p(\mathbf{r}, z) \to E_p(\mathbf{r}, z) \exp\left(-\frac{i k_0 Z_\xi}{2}\int_0^z dz' \left[\frac{d\xi}{dz'}\right]^2\right). \qquad (20)$$

Here we have introduced z-independent renormalization constants Z_ξ and Z_γ, the latter such that $\gamma \to \gamma Z_\gamma$. These are necessary since the rate of acquired phase is unknown at this stage, similar to the situation in interacting field theories [60,61]. Given a number of renormalization conditions that fix the values of the renormalization constants, the theory achieves predictive power. Here the constant Z_ξ (Z_γ) can be determined by fixing known linear (nonlinear) effects to either numerical simulations or experimental data. The renormalization constants manifest themselves as counterterms in the renormalized Lagrangian, which reads

$$L = \frac{P k_0}{2}\left(\frac{d\xi}{dz}\right)^2 - H_* + (Z_\xi - 1)\frac{P k_0}{2}\left(\frac{d\xi}{dz}\right)^2 - (Z_\gamma - 1)H_*^{(2)}, \qquad (21)$$

where $H_*^{(2)}$ is the part of the Hamiltonian containing only the nonlinearity introduced by Δn in Eq. (2). By minimizing the Lagrangian, we find the equation of motion

$$\frac{d^2\xi}{dz^2} = -\frac{1}{P k_0 Z_\xi}\frac{\partial H_*}{\partial \xi}. \qquad (22)$$

Upon renormalization, we find the constants to have values $Z_\xi = 4$ and $Z_\gamma = 0.76$. These are fixed by the initial propagation of a single low-P simulation and a single high-P simulation, respectively for Z_ξ and Z_γ. Importantly, we can now use these values for *any* P, ξ, or δ.

From Fig. 2 we can expect dynamics in the form of oscillations if the input electric-field envelope has ξ or δ slightly away from the minimum. The frequency of these oscillations can be related to the surface tension of the droplet

[2]The explicit binding energy $B_0 = -3\gamma^2 k_0^4 P^4 C_\phi^2 \log(\frac{4\gamma k_0^2 P}{\pi n_0})/2\pi^2 + \gamma^2 k_0^4 P^4 (28\delta^4 + 36\delta^2 + 28) + \gamma k_0 P/16\pi n_0 \sigma^2$.

[3]In a dipolar BEC, the stabilization mechanism is due to the Lee-Huang-Yang quantum correction term, which scales as $\rho_0^{3/2}$ as opposed to ρ_0^2 [3,11,12,14].

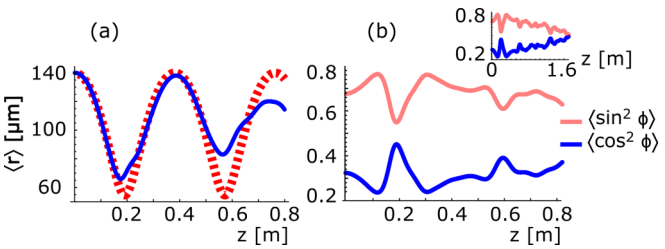

FIG. 3. (a) Evolution of the radius $\langle r \rangle$ as predicted by analytical theory (red dashed line) and direct numerical simulation (blue solid line) with initial conditions $\xi_0 = 70\ \mu$m, $|\delta| = 0.9$, and $P = 2$ W. (b) Similarly, numerical evolution of $\langle \cos^2 \phi \rangle$ [blue solid (lower) line] and $\langle \sin^2 \phi \rangle$ [red shaded (upper) line]. In the inset, droplet rotation can be seen more clearly at longer propagation distance.

[25].[4] We choose as initial conditions $\xi_0 = 70\ \mu$m and $\delta = 0.9$ with input power $P = 2$ W and evolve using a split-step propagation algorithm [56]. In Fig. 3 we show the evolution of the radius $\langle r \rangle$, $\langle \sin^2 \phi \rangle$, and $\langle \cos^2 \phi \rangle$ at different z. We observe oscillations in the radius as well as an overall rotation. The variational model is in excellent qualitative and good quantitative agreement with the exact dynamics of the system. In particular, the main feature of the evolution, i.e., oscillations in size, are properly reproduced by our model, including the correct period of the oscillations. If we further consider the angular dynamics, we see that the overall trend in Fig. 3(b) implies that the droplet is rotating and the small oscillations indicate that the angular distribution oscillates (for more details of this rotation, see the Supplemental Material, Video 1 [62]). The latter can be attributed to the system attempting to reach the $|\delta| = 1$ minimum, but due to conservation of angular momentum is only able to temporarily scatter momenta away from the bound state.

We now consider the far-from-equilibrium situation (see Fig. 4) (see also the Supplemental Material, Video 2 [62]). Here the initial condition, shown in Fig. 4(a), is a slightly perturbed vortex ($|\delta| = 0.05$) with input power $P = 15$ W. This is in the unstable regime (left of the spinodal decomposition point, i.e., where $K^{-1} \leqslant 0$) and droplet nucleation is expected. Indeed, the p-wave droplet emerges after a few violent collapse-rebound cycles. While most of the pseudoenergy is either shed or redistributed into binding energy, some excess pseudoenergy manifests itself as surface vibrations.

VII. CONCLUSION

We have found and described bound states carrying nonzero orbital angular momentum in a photon fluid with nonlocal attractive (focusing) interactions (nonlinearity). In particular, using matter-wave analogies and developing theoretical tools not typically used in optics, we found that these states are stabilized by a competition of long-range s-wave and d-wave forces, exhibit liquid behavior, and are thus a type of *droplet*. In fact, these bound states are similar to

[4]This can also be seen by calculating the surface tension as $\Sigma = \int dl[\mathcal{H}_* - \mu_* \rho_p]$, with l being the coordinate orthogonal to the surface, and compare this with the frequency of small-size excitations.

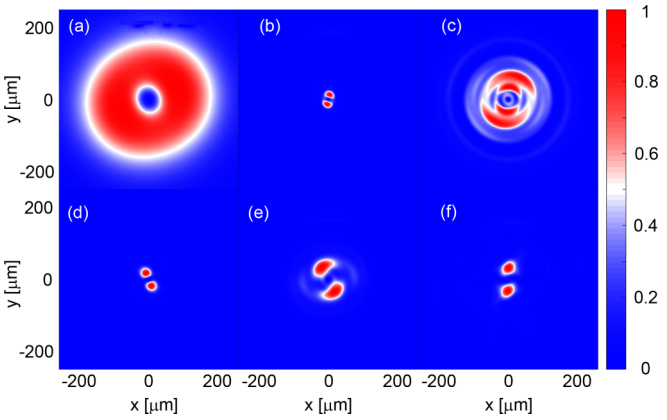

FIG. 4. Evolution snapshots for an initial power $P = 15$ W, radial size $\xi_0 = 70\ \mu$m, $|\delta| = 0.05$, and (a) $z = 0$ m, (b) $z = 0.05$ m, (c) $z = 0.075$ m, (d) $z = 0.11$ m, (e) $z = 0.13$ m, and (f) $z = 3$ m. Observe the initial collapse in (b), followed by a violent rebound in (c). This collapse-rebound cycle continues (less violently) until the system has redistributed most of its pseudoenergy into p-wave droplet binding energy, such as in (f). Excess pseudoenergy emerges as surface vibrations (see Supplemental Material, Video 2 [62]).

the droplets recently found experimentally in dipolar atomic gases, albeit with a different stabilization mechanism. The observed rotation may be linked to self-induced synthetic magnetic fields recently introduced in photon fluids [63].

ACKNOWLEDGMENTS

The authors would like to acknowledge insightful discussions with Calum Maitland, Magnus Borgh, and Luis Santos. N.W. and C.W.D. acknowledges support from EPSRC CM-CDT Grant No. EP/L015110/1. P.Ö. and M.V. acknowledge support from EPSRC Grant No. EP/M024636/1. D.F. acknowledges financial support from the European Research Council under the European Unions Seventh Framework Programme Grant No.ERC GA 306559 and EPSRC (UK) Grant No. EP/P006078/2.

APPENDIX A: VALIDITY OF THE LWA

A commonly used expansion for a nonlocal refractive index is the so-called Snyder-Mitchell approximation, where the refractive index is simply proposed to take the form of a parabola [27]. This would correspond to only keeping the s-wave term of the above expansion and further approximating the medium's response function $R(\mathbf{r}) \propto r^2$. Let us now examine the regions of validity of the long-wavelength approximation and compare this to the Snyder-Mitchell approach. Note that we will show that the Snyder-Mitchell approach is incorrect for nonzero OAM in Appendix B. We start from Eq. (2), which gives the thermally induced refractive-index change from the distributed loss model as

$$\Delta n(\mathbf{r}, z) = \gamma \int d^2 r' R(\mathbf{r} - \mathbf{r}') |E(\mathbf{r}', z)|^2, \qquad \text{(A1)}$$

with $|E(\mathbf{r}, z)|^2$ scaled such that it yields the transverse intensity profile. As an illustrative example we use the case of a spherically symmetric (s-wave) Gaussian of power P and spot

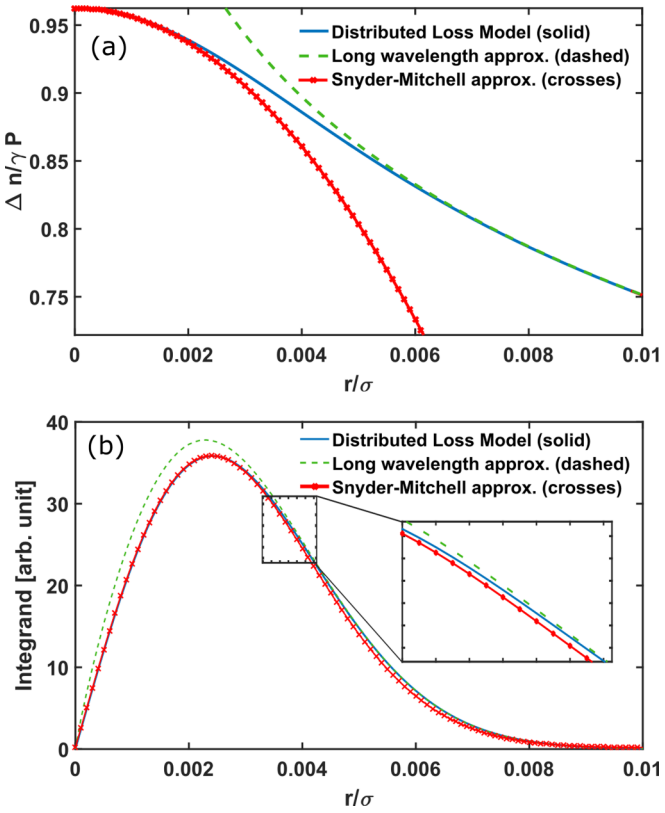

FIG. 5. (a) Scaled index change $\Delta n/\gamma P$ versus r/σ according to the long-wavelength approximation (A4) (dashed line), according to the Snyder-Mitchell approximation (A5) (solid line with crosses), and the exact index change (solid line). (b) Exact solution for $\Delta n(r)$ (solid line), the long-wavelength approximation (dashed line), and the Snyder-Mitchell approximation (solid line with crosses). Notice that the different approximate refractive-index profiles both give similar integrands. One should note that a p-wave droplet is expected to be localized at radii $r \gtrsim 0.0035\sigma$, where the long-wavelength approximation better approximates the distributed loss model. The inset shows the crossover region.

size ξ,

$$|E(\mathbf{r}, z)|^2 = \frac{2P}{\pi\xi^2} e^{-2r^2/\xi^2}. \tag{A2}$$

For such a symmetric intensity profile the refractive-index profile may be recast in cylindrical coordinates as

$$\Delta n(r, z) = \gamma \int_0^\infty |E(\zeta, z)|^2 G_0(r, \zeta; a)\zeta \, d\zeta, \tag{A3}$$

where the Green's function is given by Eq. (7) of Ref. [64], but where in their notation $\zeta \to \xi$ and W denotes the spot size instead of ξ. In our case, the parameter a is equal to the nonlocal length σ.

We are interested in the case when the Gaussian spot size is much smaller than the nonlocal length $\xi \ll \sigma$ and we set $\xi = 0.005\sigma$ as an example. The solid line in Fig. 5(a) shows the scaled index change $\Delta n/\gamma P$ versus r/σ calculated numerically according to Eq. (A3) above and we will use this example as a test bed for the approximations employed in the paper.

The long-wavelength approximation is given by Eq. (17) and this yields

$$\frac{\Delta n}{\gamma P} = \frac{K_0(r/\sigma)}{2\pi\sigma^2}\left[1 + \frac{1}{2}\left(\frac{\xi}{\sigma}\right)^2\right], \tag{A4}$$

We note that this approximation for the scaled index change $\Delta n/\gamma P$ does not involve the Gaussian spot size. This arises since the narrow Gaussian with $\xi \ll \sigma$ acts like a δ function multiplied by the power P. The dashed line in Fig. 5(a) shows the scaled index change $\Delta n/\gamma P$ versus r/σ according to the long-wavelength approximation Eq. (A4). We see, as expected, that the long-wavelength approximation does not work well near the origin but it improves at larger distances. For the p-wave case discussed in the text, the centrifugal barrier makes the droplets avoid short distances, as we have seen, and short distances become irrelevant.

We will discuss the Snyder-Mitchell model in more detail in Appendix B, but in short the thermally induced refractive-index change is given by

$$\Delta n(r) - \Delta n(0) = -\frac{\gamma P}{4\sigma^2 A_{\text{eff}}} r^2, \tag{A5}$$

where $A_{\text{eff}} = \pi\xi^2/2$ for the Gaussian example and $\Delta n(0)$ is the on-axis index change. The solid line with crosses in Fig. 5(a) shows the scaled index change $\Delta n/\gamma P$ versus r/σ according to the Snyder-Mitchell approximation (A5). In contrast to the long-wavelength approximation, the Snyder-Mitchell approximation works very well close to the origin but deviates at larger distances. In particular, the Snyder-Mitchell approximation provides a better approximation to the index profile for distances $r \lesssim \xi/\sqrt{2} = 0.0035\sigma$, which is over the spatial extent of the Gaussian example of width ξ. While the on-axis Gaussian provides an illustrative example, we should note that p-wave droplet is localized off-axis. In fact, we expect the peaks and thus the bulk of the field intensity to be at radii $r \gtrsim \xi/\sqrt{2}$ and thus the long-wavelength approximation is preferred.

An apparent issue arises in that we are using noticeably different forms of the scaled index change $\Delta n/\gamma P$ from the long-wavelength approximation and the Snyder-Mitchell approximation but hoping to address the same physics. The question is how useful information may be obtained based on the long-wavelength approximation which actually diverges near the origin. The answer lies in the fact that we use the LWA in a variational (Lagrangian or Hamiltonian) calculation that involves the integral of the refractive index profile and the intensity of the form

$$\int_0^\infty \underbrace{|E(r)|^2 \Delta n(r) r}_{\text{integrand}} \, dr. \tag{A6}$$

In Fig. 5(b) we plot the underbraced integrand versus r/σ from this integral for the exact solution for $\Delta n(r)$ (solid line), the long wavelength approximation (dashed line), and the Snyder-Mitchell approximation (solid line with crosses). Here we see that, despite the differences in the approximate refractive-index profiles, they give very similar results for the integrand. Thus, from the perspective of the variational methods, the different approaches should yield similar results in

the spherically symmetric case since they depend on integrals as above.

APPENDIX B: COMPARISON TO THE SNYDER-MITCHELL APPROXIMATION

We will here explore the p-wave droplet characteristics under the assumption that the Snyder-Mitchell model of the nonlocal response function is correct. There is a plethora of Snyder-Mitchell models, many of which assume a constant harmonic frequency [27–29,36,42,65]. These models are azimuthally symmetric and droplet-shape independent, so it comes as no surprise that the pseudoenergy is δ independent. However, we can improve upon this by taking the shape into account. As before, let us start at the paraxial wave equation

$$i\frac{\partial E(\mathbf{r},z)}{\partial z} = -\frac{1}{2k_0}\nabla^2 E(\mathbf{r},z) - \frac{k_0}{n_0}\Delta n(\mathbf{r},z)E(\mathbf{r},z). \quad \text{(B1)}$$

In the Snyder-Mitchell regime, the nonlocal response of the medium is approximated as $\Delta n(\mathbf{r}) \simeq -\Omega^2 r^2$, where Ω is the harmonic-oscillator frequency given by the relation

$$\Omega^2 = \frac{\alpha\beta P}{4\kappa A_{\text{eff}}} = \frac{\gamma P}{4\sigma^2 A_{\text{eff}}} \quad \text{(B2)}$$

and where

$$A_{\text{eff}} = \frac{\left(\int d^2r|E(\mathbf{r})|^2\right)^2}{\int d^2r|E(\mathbf{r})|^4} \quad \text{(B3)}$$

is the effective area of the beam. We are looking for droplets with orbital angular momentum $\ell \neq 0$ and thus we make the *Ansatz*

$$E(\mathbf{r},z) = E_d(\mathbf{r})e^{i\ell\phi}e^{-i\mu_* z}. \quad \text{(B4)}$$

This has solutions of the form

$$E_p(r,\phi) = r^{|\zeta|}{}_1F_1(-n,|\zeta|+1,2r^2/\xi^2)e^{-r^2/\xi^2}e^{im\phi}, \quad \text{(B5)}$$

where m is an integer, n is a positive integer, $|\zeta| = |m+\ell|$, and ${}_1F_1$ is the confluent hypergeometric function of the first kind. The pseudochemical potential of this family of solutions is given by

$$\mu_* = \frac{k_0\gamma P}{4n_0 C_{\text{area}}\sigma^2}(2n+|\zeta|+1). \quad \text{(B6)}$$

Here we have defined $C_{\text{area}} \equiv A_{\text{eff}}/\xi^2$. Focusing on the case of $n=0$, the normalized droplet takes the form

$$E_d(r,\phi) = \frac{2^{(|\zeta|+1)/2}\sqrt{P}\xi^{(-2|\zeta|-2)/2}}{\sqrt{\pi}\sqrt{\Gamma(|\zeta|+1)}} \times r^{|\zeta|}{}_1F_1(0,|\zeta|+1,2r^2/\xi^2)e^{-r^2/\xi^2}e^{\pm im\phi}.$$

For this to be a self-consistent solution, we require that

$$\frac{4}{\xi^4} = \frac{2k_0^2\Omega^2(\xi)}{n_0} \quad \text{(B7)}$$

and thus

$$\frac{4}{\xi^4} = \frac{2k_0^2\gamma P}{4\sigma^2 A_{\text{eff}}(\xi)} = \frac{2k_0^2\gamma P}{4n_0\sigma^2 C_{\text{area}}\xi^2}, \quad \text{(B8)}$$

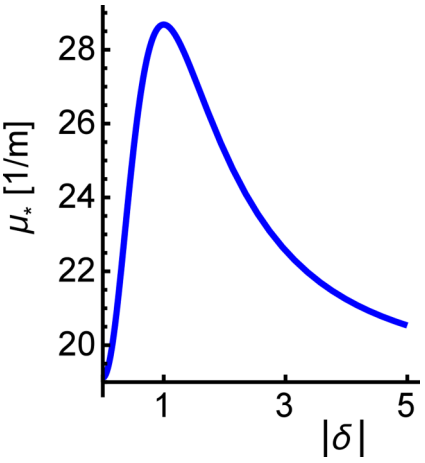

FIG. 6. Pseudochemical potential surface of the droplet as a function of the variational parameter δ as given by Eq. (B6) from the Snyder-Mitchell model with $P = 1$W. As can be seen, this energy landscape is qualitatively different from the one seen in Fig. 2(a). This is also qualitatively different from numerical evidence.

where in the latter step we used Eq. (B3) to calculate the effective area. In the above,

$$C_{\text{area}} = \frac{4^{|\zeta|}\Gamma(|\zeta|+1)^2\pi}{\Gamma(2|\zeta|+1)}. \quad \text{(B9)}$$

Solving the self-consistency relation for the characteristic size ξ yields

$$\xi = \sqrt{\frac{8C_{\text{area}}n_0}{k_0^2\gamma P}}\sigma. \quad \text{(B10)}$$

So far, this looks quite far from the observed p-wave droplet. However, let us look closer at the pseudochemical potential μ_*. If we let $\ell = 1$, then we notice that $m = 0$ and $m = -2$ both have $|\zeta| = 1$. Therefore, the $m = 0$ and $m = -2$ state has the same pseudoenergy. In other words, the ground state is degenerate. We can now form a superposition of s- and d-wave states (for OAM $\ell = 1$) as a superpositon of the two degenerate ground states, i.e., the electric field takes the form

$$E_d^{p\text{ wave}}(r,\phi) = \frac{2\sqrt{P}}{\sqrt{\pi}\sqrt{1+\delta^2}\xi^2}re^{-r^2/\xi^2}[1+\delta e^{-2i\phi}]. \quad \text{(B11)}$$

Here we should point out that in general a superposition has a different effective area than either of its constituents, that is, the area is not given by Eq. (B9) in general and thus the pseudochemical potential will vary with δ. The pseudochemical potential and the pseudoenergy are connected through Eq. (10), therefore the landscape of the pseudochemical potential maps directly to the pseudoenergy surface. In Fig. 6 we see that the Snyder-Mitchell model predicts qualitatively different behavior than the low-wavelength approximation (cf. Fig. 2). The long-wavelength approximation is in agreement with numerical results; we must conclude that the Snyder-Mitchell model is not sufficient to capture the physics addressed in this work.

[1] F. Dalfovo, A. Lastri, L. Pricaupenko, S. Stringari, and J. Treiner, Phys. Rev. B **52**, 1193 (1995).

[2] I. Ferrier-Barbut, H. Kadau, M. Schmitt, M. Wenzel, and T. Pfau, Phys. Rev. Lett. **116**, 215301 (2016).

[3] M. Schmitt, M. Wenzel, F. Böttcher, I. Ferrier-Barbut, and T. Pfau, Nature (London) **539**, 259 (2016).

[4] C. R. Cabrera, L. Tanzi, J. Sanz, B. Naylor, P. Thomas, P. Cheiney, and L. Tarruell, Science **359**, 301 (2018).

[5] P. Cheiney, C. R. Cabrera, J. Sanz, B. Naylor, L. Tanzi, and L. Tarruell, Phys. Rev. Lett. **120**, 135301 (2018).

[6] H.-W. Hammer and D. T. Son, Phys. Rev. Lett. **93**, 250408 (2004).

[7] B. Bazak and D. S. Petrov, New J. Phys. **20**, 023045 (2018).

[8] H. Kadau, M. Schmitt, M. Wenzel, C. Wink, T. Maier, I. Ferrier-Barbut, and T. Pfau, Nature (London) **530**, 194 (2016).

[9] L. Chomaz, S. Baier, D. Petter, M. J. Mark, F. Wächtler, L. Santos, and F. Ferlaino, Phys. Rev. X **6**, 041039 (2016).

[10] R. Schützhold, M. Uhlmann, X. Yan, and U. R. Fischer, Int. J. Mod. Phys. B **20**, 3555 (2006).

[11] F. Wächtler and L. Santos, Phys. Rev. A **93**, 061603(R) (2016).

[12] F. Wächtler and L. Santos, Phys. Rev. A **94**, 043618 (2016).

[13] I. Ferrier-Barbut, M. Schmitt, M. Wenzel, H. Kadau, and T. Pfau, J. Phys. B **49**, 214004 (2016).

[14] R. N. Bisset, R. M. Wilson, D. Baillie, and P. B. Blakie, Phys. Rev. A **94**, 033619 (2016).

[15] D. S. Petrov, Phys. Rev. Lett. **115**, 155302 (2015).

[16] A. Bulgac, Phys. Rev. Lett. **89**, 050402 (2002).

[17] M. Valiente and P. Öhberg, Phys. Rev. A **94**, 051606(R) (2016).

[18] K. S. Krane, *Introductory Nuclear Physics*, 3rd ed. (Wiley, New York, 1987).

[19] F. Dalfovo and S. Stringari, J. Chem. Phys. **115**, 10078 (2001).

[20] A. Almand-Hunter, H. Li, S. Cundiff, M. Mootz, M. Kira, and S. Koch, Nature (London) **506**, 471 (2014).

[21] S. Burger, K. Bongs, S. Dettmer, W. Ertmer, K. Sengstock, A. Sanpera, G. V. Shlyapnikov, and M. Lewenstein, Phys. Rev. Lett. **83**, 5198 (1999).

[22] J. Denschlag, J. Simsarian, D. Feder, C. W. Clark, L. Collins, J. Cubizolles, L. Deng, E. W. Hagley, K. Helmerson, W. P. Reinhardt *et al.*, Science **287**, 97 (2000).

[23] P. G. Kevrekidis, D. J. Frantzeskakis, and R. Carretero-González, *Emergent Nonlinear Phenomena in Bose-Einstein Condensates: Theory and Experiment* (Springer Science + Business Media, New York, 2007), Vol. 45.

[24] G. I. Stegeman and M. Segev, Science **286**, 1518 (1999).

[25] H. Michinel, J. Campo-Táboas, R. García-Fernández, J. R. Salgueiro, and M. L. Quiroga-Teixeiro, Phys. Rev. E **65**, 066604 (2002).

[26] H. Michinel, M. J. Paz-Alonso, and V. M. Pérez-García, Phys. Rev. Lett. **96**, 023903 (2006).

[27] A. W. Snyder and D. J. Mitchell, Science **276**, 1538 (1997).

[28] O. Bang, W. Krolikowski, J. Wyller, and J. J. Rasmussen, Phys. Rev. E **66**, 046619 (2002).

[29] C. Conti, M. Peccianti, and G. Assanto, Phys. Rev. Lett. **92**, 113902 (2004).

[30] X. Hutsebaut, C. Cambournac, M. Haelterman, A. Adamski, and K. Neyts, Opt. Commun. **233**, 211 (2004).

[31] Z. Xu, Y. V. Kartashov, and L. Torner, Opt. Lett. **30**, 3171 (2005).

[32] D. Mihalache, D. Mazilu, F. Lederer, B. A. Malomed, Y. V. Kartashov, L.-C. Crasovan, and L. Torner, Phys. Rev. E **73**, 025601(R) (2006).

[33] Y. J. He, B. A. Malomed, D. Mihalache, and H. Z. Wang, Phys. Rev. A **77**, 043826 (2008).

[34] C. Rotschild, T. Schwartz, O. Cohen, and M. Segev, Nat. Photon. **2**, 371 (2008).

[35] B. K. Esbensen, M. Bache, O. Bang, and W. Krolikowski, Phys. Rev. A **86**, 033838 (2012).

[36] W.-P. Zhong, M. R. Belić, and T. Huang, Nonlinear Dyn. **70**, 2027 (2012).

[37] N. B. Aleksić, M. S. Petrović, A. I. Strinić, and M. R. Belić, Phys. Rev. A **85**, 033826 (2012).

[38] G. Liang and Q. Guo, Phys. Rev. A **88**, 043825 (2013).

[39] D. Lu, Q. Zhan, Q. Duan, and W. Hu, Phys. Rev. A **87**, 023815 (2013).

[40] H. Zhang, F. Xu, D. Zhu, L. Zhang, D. Xu, and Y. Tian, Opt. Express **22**, 995 (2014).

[41] G. Liang, Q. Guo, W. Cheng, N. Yin, P. Wu, and H. Cao, Opt. Express **23**, 24612 (2015).

[42] A. Alberucci, C. P. Jisha, and G. Assanto, J. Opt. **18**, 125501 (2016).

[43] M. Peccianti, K. A. Brzdkiewicz, and G. Assanto, Opt. Lett. **27**, 1460 (2002).

[44] C. Rotschild, M. Segev, Z. Xu, Y. V. Kartashov, L. Torner, and O. Cohen, Opt. Lett. **31**, 3312 (2006).

[45] S. Lopez-Aguayo, A. S. Desyatnikov, Y. S. Kivshar, S. Skupin, W. Krolikowski, and O. Bang, Opt. Lett. **31**, 1100 (2006).

[46] Y. V. Izdebskaya, A. S. Desyatnikov, G. Assanto, and Y. S. Kivshar, Opt. Express **19**, 21457 (2011).

[47] N. Schine, A. Ryou, A. Gromov, A. Sommer, and J. Simon, Nature (London) **534**, 671 (2016).

[48] A. Amo, J. Lefrère, S. Pigeon, C. Adrados, C. Ciuti, I. Carusotto, R. Houdré, E. Giacobino, and A. Bramati, Nat. Phys. **5**, 805 (2009).

[49] A. Amo, S. Pigeon, D. Sanvitto, V. Sala, R. Hivet, I. Carusotto, F. Pisanello, G. Leménager, R. Houdré, E. Giacobino *et al.*, Science **332**, 1167 (2011).

[50] D. Sanvitto, S. Pigeon, A. Amo, D. Ballarini, M. De Giorgi, I. Carusotto, R. Hivet, F. Pisanello, V. Sala, P. Guimaraes *et al.*, Nat. Photon. **5**, 610 (2011).

[51] G. Nardin, G. Grosso, Y. Léger, B. PiÈtka, F. Morier-Genoud, and B. Deveaud-Plédran, Nat. Phys. **7**, 635 (2011).

[52] A. Minovich, D. N. Neshev, A. Dreischuh, W. Krolikowski, and Y. S. Kivshar, Opt. Lett. **32**, 1599 (2007).

[53] D. Vocke, T. Roger, F. Marino, E. M. Wright, I. Carusotto, M. Clerici, and D. Faccio, Optica **2**, 484 (2015).

[54] D. Vocke, K. Wilson, F. Marino, I. Carusotto, E. M. Wright, T. Roger, B. P. Anderson, P. Öhberg, and D. Faccio, Phys. Rev. A **94**, 013849 (2016).

[55] R. W. Boyd, *Nonlinear Optics* (Academic, New York, 2003).

[56] T. Roger, C. Maitland, K. Wilson, N. Westerberg, D. Vocke, E. M. Wright, and D. Faccio, Nat. Commun. **7**, 13492 (2016).

[57] H. Smith and C. J. Pethick, *Bose-Einstein Condensation in Dilute Gases* (Cambridge University Press, Cambridge, 2001).

[58] R. Machleidt and D. R. Entem, Phys. Rep. **503**, 1 (2011).

[59] P. M. Chaikin and T. C. Lubensky, *Principles of Condensed Matter Physics* (Cambridge University Press, Cambridge, 2000), Chap. 8.7.

[60] M. Srednicki, *Quantum Field Theory* (Cambridge University Press, Cambridge 2007).
[61] T. Lancaster and S. J. Blundell, *Quantum Field Theory for the Gifted Amateur* (Oxford University Press, Oxford, 2014).
[62] See Supplemental Material at http://link.aps.org/supplemental/10.1103/PhysRevA.98.053835 for videos.
[63] N. Westerberg, C. Maitland, D. Faccio, K. Wilson, P. Öhberg, and E. M. Wright, Phys. Rev. A **94**, 023805 (2016).
[64] A. I. Yakimenko, Y. A. Zaliznyak, and Y. Kivshar, Phys. Rev. E **71**, 065603(R) (2005).
[65] A. Alberucci, C. P. Jisha, N. F. Smyth, and G. Assanto, Phys. Rev. A **91**, 013841 (2015).